Sensors and Materials, Vol. 36, No. 8 (2024) 3479–3490
MYU Tokyo

S & M 3746

Crack Nucleation and Propagation Mechanisms of Sputtered AlSi Alloy Thin Film under Quasistatic and Dynamic Tension

Takahiro Namazu,[1*] Ginnosuke Ina,[2] Hiroki Tsuma,[3] and Tsuyoshi Nishiwaki[3]

[1]Kyoto University of Advanced Science, 18 Yamanouchigotanda-cho, Ukyo, Kyoto 615-8577, Japan
[2]University of Hyogo, 2167 Shosha, Himeji, Hyogo 671-2280, Japan
[3]MIRISE Technologies Corporation,
500-1 Minamiyama, Komenoki-cho, Nisshin, Aichi 470-0111, Japan

(Received July 16, 2024; accepted August 6, 2024)

Keywords: AlSi alloy thin film, sputtering, tensile test, fatigue test, crack nucleation, crack propagation, Si segregation, degradation

In this study, we examined the fatigue crack nucleation and propagation mechanisms of an AlSi sputtered thin film subjected to the quasistatic tensile test and cyclic loading test by scanning electron microscopy. An AlSi thin film with 1.0 wt% Si was prepared by dc magnetron sputtering at a substrate temperature of 260 °C, followed by annealing at 490 °C. Two types of uniaxial tensile test equipment were prepared, namely, manual tensile loading equipment and automatic tensile loading equipment. The combination of the use of manual-type equipment and electron backscattered diffraction analysis enabled us to visualize crystal grain subdivision mechanisms. The automatic-type equipment enabled us to understand fatigue crack propagation mechanisms in the AlSi thin film after crack nucleation originating from grain subdivision. A fatigue crack propagated in a zigzag manner under the low stress amplitude condition during the fatigue test, whereas it propagated straightly under the high stress amplitude condition. This phenomenon is discussed from the viewpoints of crack detouring around Si segregates and Si brittleness.

1. Introduction

Owing to their low electric resistance, high strength-to-weight ratio, nonbrittle characteristic, and ease of deposition by sputtering and vacuum evaporation, pure Al and Al alloy films are commonly used as wiring and structural materials in various semiconductor and MEMS devices.[1–5] In the dry processes to deposit Al-related films, it is easy to include additive elements into the Al film. A certain amount of an additive element can be contained in the target, so film composition can be precisely controlled. In the case of 3D MEMS structures made of an Al alloy film, the mechanical characteristics of the film should be examined experimentally to improve its performance and reliability. A uniaxial tensile test directly

*Corresponding author: e-mail: namazu.takahiro@kuas.ac.jp
https://doi.org/10.18494/SAM5240

ISSN 0914-4935
https://myukk.org/

measures the mechanical properties of a thin film if a sophisticated evaluation technique is prepared.[6–13] A dynamic uniaxial tensile test is important for investigating fatigue characteristics against cycling external loading. As examples of studies of the fatigue test of Al alloy films, Barrios *et al.* developed a system for the high-throughput fatigue test to investigate fatigue cracking in sputtered Al films.[14] They showed that fatigue cracks exhibited significant tortuosity and tended to follow hillocks on the Al film surface. Koike *et al.* discussed in detail fatigue cracking and deformation mechanisms in sputtered AlSi films during a thermal cycling test.[15] On the basis of the microstructural observation after the test, they demonstrated that the initial increase in the amount of residual stress was caused by the increase in the amount of lattice dislocations and their tangling, and the following decrease in the amount of residual stress was caused by crack formation and delamination. Shindo *et al.* demonstrated the effectiveness of a Si additive into the Al film for the extension of lifetime in the AlSi film.[16] Understanding of fatigue mechanisms including fatigue crack nucleation and propagation during cyclic loading enables us to design semiconductor and MEMS devices with high performance and reliability.[17]

The objective of this research is to experimentally characterize the degradation of sputtered AlSi thin film under cyclic loading. In particular, we focus on clarifying crack initiation and propagation under quasistatic uniaxial tension loading and dynamic tension loading while observing crystal grain degradation and cracking around Si segregates by electron backscattered diffraction (EBSD) and energy dispersive X-ray (EDX) analyses, respectively. Lastly, the influence of stress amplitude during the fatigue test on fatigue cracking is discussed.

2. Experimental Procedure

Figure 1 shows a photograph of the tensile test specimen produced using conventional semiconductor fabrication technologies. First, a 4-inch n-type Si (001) wafer of 300 μm thickness was oxidized under wet thermal conditions at 1100 °C for 2 h to grow a 1-μm-thick amorphous Si oxide (SiO_x) film on the entire wafer. On the top surface, an AlSi alloy film of 5 μm thickness was deposited by dc magnetron sputtering using an AlSi alloy target with a Si content of 1.0 wt%. The substrate temperature during sputtering was kept constant at 260 °C. After the deposition, annealing was conducted at 490 °C in a hydrogen + nitrogen atmosphere for 1 h.

After annealing, a dog-bone-shaped self-standing monolayer film specimen for the tensile mode fatigue test was produced using conventional micromachining processes. The specimen shape was patterned onto the deposited film by a photolithography technique, followed by wet etching with a mixed solution of phosphoric acid, nitric acid, and acetic acid. As shown in the enlarged photograph in Fig. 1, a free-standing monolayer film specimen consists of a parallel section and a curvature section. At the boundary between the two sections, four isosceles triangles each measuring approximately 7 μm in height and 10 μm in bottom width were made, which are used as gauge marks to measure specimen elongation during tensile tests.[16] The length and width of the parallel section were set to be 500 and 200 μm, respectively. After the specimen section fabrication, through holes were made by photolithography and a dry etching method, called deep reactive-ion etching (DRIE) from the back side of a wafer. Through DRIE

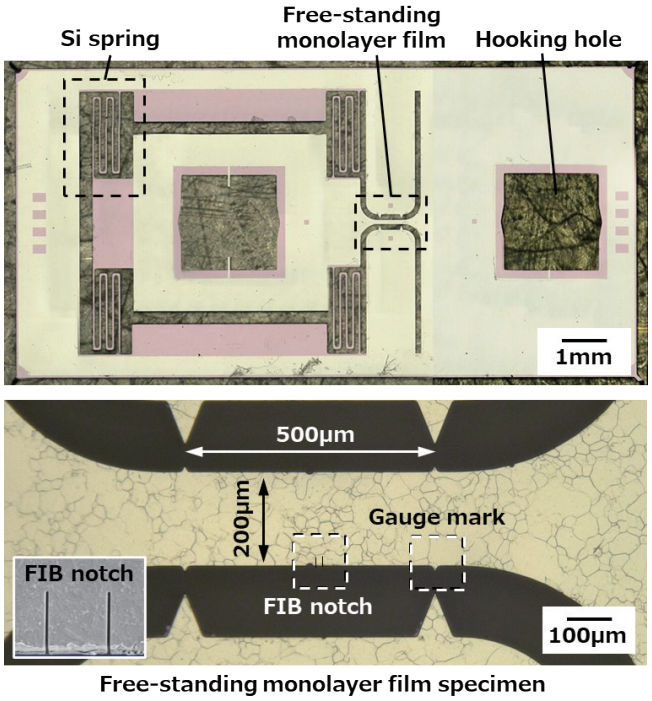

Fig. 1. (Color online) Photograph of AlSi film specimen for quasistatic and dynamic tension loading.

with the BOSCH process recipe using sulfur hexafluoride (SF_6) and octafluorocyclobutane (C_4F_8) gases, two square holes, four Si springs, and a space beneath a film specimen were formed. After the etching, one end of the specimen section, which is the portion supported by four Si springs, became movable. The spring width was only 100 μm, and a film specimen was easily deformed along the tensile direction only, so no misalignment between the specimen's longitudinal direction and the tensile direction happened during the tensile test. The square holes were used for hooking vertical rectangular solid pins installed in the tensile test apparatus to apply a tensile force. The space beneath a film specimen makes the film in the tension section free-standing. A film in the dog-bone section exists as a self-standing monolayer, whereas the film in other portions exists as the double layers of the film and substrate. Lastly, after the SiO_x layer on the back side of a film specimen was completely removed by wet etching with buffered hydrofluoric acid, the preparation of the tensile test specimen was completed.

For crystal grain degradation evaluation under quasistatic tension, double notches at the center of the specimen parallel section were fabricated using a focused ion beam (FIB). The length and width of each notch were 25 and 2 μm, respectively, and the distance between the two was 20 μm. For crack propagation evaluation under dynamic tension, no notches were introduced into the films.

Figure 2 shows photographs of the uniaxial tensile test equipment for thin film evaluation. Two types of uniaxial tensile test equipment were prepared, namely, manual tensile loading equipment and automatic tensile loading equipment. The manual-type equipment, which was specially designed for crystal grain degradation observation at the tip of a notch using EBSD,

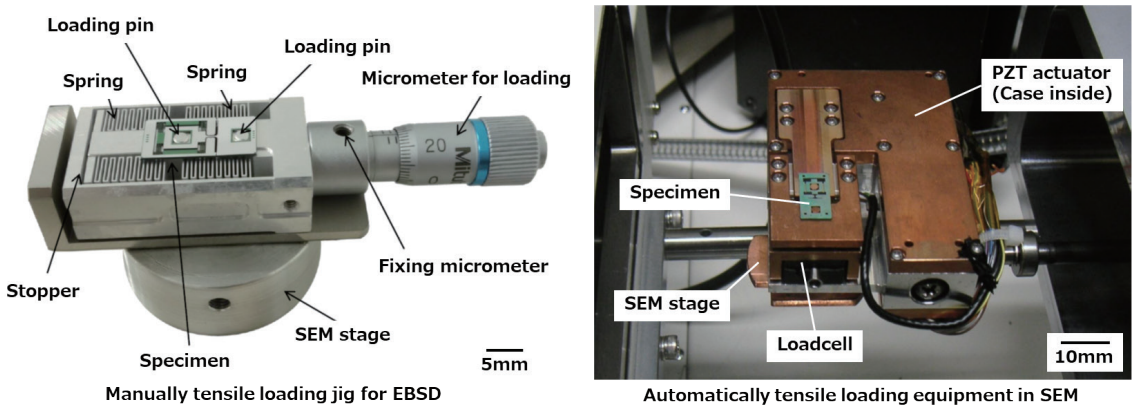

Fig. 2. (Color online) Tensile test equipment for quasistatic and dynamic tension loading.

consists of a sample stage with two hooking pins, a spring structure, a micrometer, and a SEM stage. The equipment is set on the stage of a commercial SEM system (ZEISS, Ultla 55 SEM) and can apply quasistatic tensile loading to a film specimen by rotating a micrometer because the two pins are manually moved away from each other. Another micrometer is set outside the SEM system, which is connected to the micrometer equipped with the manual-type jig via a flexible tube. The automatic-type equipment was designed and developed to be of compact size, which enables us to conduct pulsating-tension cyclic loading tests in a SEM system (Hitachi High-Tech, S4800 Type II). The equipment is composed of a piezoelectric actuator for automatic quasistatic/dynamic tensile force application, a load cell, a course moving stage, a SEM holder, a pair of sample holders with a square vertical pin for hooking a specimen, and an actuator case with a lever structure to amplify a PZT actuator's elongation by a factor of 4.1 along the tensile direction. By setting the equipment into the SEM system, it can be operated using a personal computer outside of the SEM system. The system enabled us to do automatic pulsating-tension fatigue tests inside the SEM system.

By using a specimen and automatic-type equipment, the pulsating tension mode fatigue test was carried out in a high vacuum in the SEM system. The frequency was set to be 10 Hz. A sinusoidal waveform was applied to the specimen and the amplitude was set on the basis of a reference stress value derived from quasistatic tensile tests.[16]

3. Results and Discussion

Figure 3 shows representative SEM images around notch tips under quasistatic uniaxial tension along with EBSD maps and its experimental setup and color definition. EBSD is known as an effective analysis tool to deeply understand the crystallinity and degradation of grains.[13,16,18] In the EBSD analysis, the inverse pole figure (IPF) distribution in the specimen's axial direction (AD), width direction (WD), and normal direction (ND) were obtained. Here, to mainly investigate the influence of axial tensile loading on crystal grain deformation and degradation around notches, we used the AD IPF data only. Although the data were omitted in this paper, all the AlSi films evaluated had a highly (111) preferred orientation in ND and a

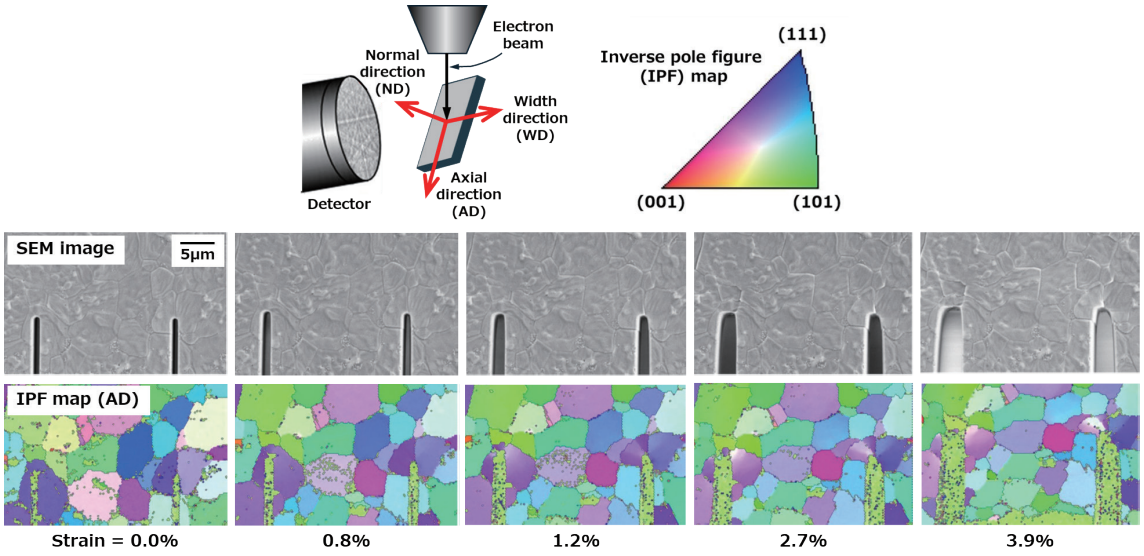

Fig. 3. (Color online) SEM and EBSD images of area around notch tip under quasistatic tension.

random orientation in AD and WD. The strain shown beneath each figure was calculated on the basis of the elongation of the parallel section measured using the two-gauge marks in the tensile direction. The tips of the notches on the left and right sides were artificially made inside a crystal grain and on the crystal grain boundary, respectively. Before applying tension, it is found from the ESBD images that the crystal grains are randomly arranged in-plane. Even when a strain of 0.8% was applied, no significant change can be seen in the SEM image, although the width of each notch was slightly enlarged. In the EBSD map, no significant change can be seen as well, except at the tip of the left-side notch. It is found that the color of the left side of the notch is changed to slightly darker than that of the right side. This indicates that the crystal grain around the notch degraded slightly. When applying tension up to 1.2%, although the notches appear clearly widened, it is difficult to find changes in the SEM image. In the EBSD map, however, two apparent changes can be found. The first change is on the tip of the left notch. One crystal grain looks divided into three different grains. The second change is on the tip of the right notch, which was made on the boundary of the two grains. Each grain consists of multiple colors. The left-side grain looks divided into three colors at the inclined angles of around 30° and 70° from the vertical line (grain boundary). The right-side grain looks divided into two colors at the angle of around 45°. This implies that shear deformation at around the tip of the notches happened in each grain and the grain subdivision started. At a tensile strain of 2.7%, it is found that the grain around the left-side notch was completely separated into at least two grains. In the grains around the right-side notch, grain subdivision was proceeding because the difference in color in each grain, that is, the subgrain boundary, became clearer than at 0.8% tensile strain. At 3.9% tensile strain, it is found that the left-side grain around the right-side notch was subdivided into three or four grains and the right-side grain was subdivided into two grains. By summarizing the EBSD analysis results obtained here, we found that the crystal in a grain around a notch tip rotated partially owing to shear deformation, and then a subgrain boundary was made along the shear

deformation direction. With increasing tensile strain, the grain subdivision proceeded continuously. Crack nucleation is expected to form around a notch, i.e., a stress-concentrated portion, after the grain subdivision happened, and the crack will propagate along the shear direction.

Figure 4 shows representative SEM images of the degraded portion taken during cyclic tensile loading. The fatigue test was carried out at a stress amplitude of 35 MPa. The SEM images until 150400 cycles were taken around the edge of the AlSi film where degradation happened, and the last two images were taken such that the entire film was covered. At 16000 cycles, multiple slip lines can be seen on the AlSi film surface. The angle of the slip lines was around 60° from the axial direction of the film specimen. At 50000 cycles, crack nucleation was formed at the edge of the film. Although it is difficult to directly see in the SEM image, it can be considered that grain subdivision happened just before the crack initiation occurred. At 105000 cycles, a crack was found to start propagating along the slip lines. The crack propagated across multiple slip lines, but it can be seen that up to 145000 cycles, the direction of propagation does not differ significantly from the direction of the slip lines. However, at 150000 cycles, the crack changed its propagation direction from top right to top left at the portion indicated by a dashed circle. At 150400 cycles, the crack became large and opened, and then it rapidly propagated into the specimen width direction up to 150800 cycles. The degradation of area A is discussed later in detail. After that, the crack slightly changed its propagation position to the left side, then propagated to the top side rapidly, leading to catastrophic fatigue failure.

In the fatigue cracking phenomena shown in Fig. 4, several interesting findings were obtained. The first one is that fatigue cracking was initiated where a dislocation glide occurred. After tensile load application, crystal grains at the stress concentration area degraded, and grain subdivision took place. Slip lines were produced owing to the degradation inside the grains. As a result, crack nucleation probably newly formed in the dense slip line portion, leading to fatigue cracking. The second one is that at the beginning of the cyclic loading test, a crack propagated

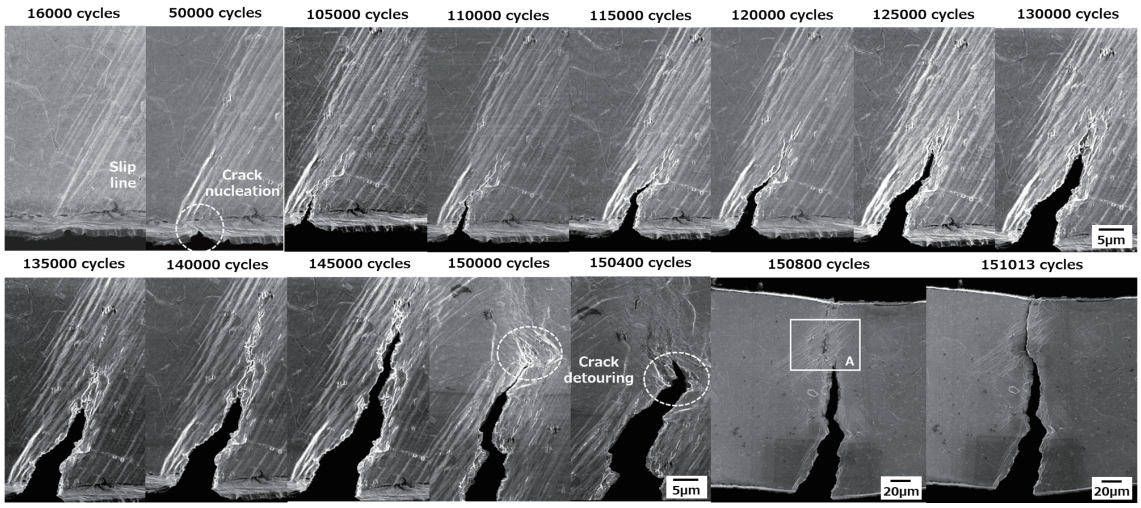

Fig. 4. SEM images of fatigue cracks in AlSi thin film under dynamic tension.

along the slip lines that appeared in advance. This indicates that the dislocation glide would have influenced the crack propagation. That is, it can be said that the dislocation glide formed the crack propagation path. The third one is that a crack changed its propagation direction suddenly. A crack propagated in a slightly zigzag manner at the beginning of the test. Then, it changed its direction considerably in the middle of the test. Figure 5(a) is the SEM image showing multiple slip lines, which are the evidence that a dislocation glide occurred. Most of the slip lines faced the same direction (in this case, from the bottom left to the top right). Some of the slip lines were formed in a different direction, which provided cross slips in the crystal grain. Note that there are several areas where no slip lines could be detected in the SEM image. According to the EDX map of the same region, the Si element shown in red was detected in the areas without slip lines. That is, it can be said that Si segregates prevented dislocation glides during the cyclic loading test. Figure 5(b) shows that there were some relationships between cracking and Si segregation. Namely, when the crack propagated in front of the Si segregates, it probably stopped for a short time and then detoured to prevent hitting the segregates.[16] Si segregates worked well to prevent cracking inside the AlSi film, which contributed to the extension of the lifetime of the Al alloy film including the Si additive. The fourth one is that the degradation of the film including dislocation glides and local cracks occurred ahead of a crack. As seen in the SEM images in Fig. 6, which are the enlarged images of area A in Fig. 4, a mottle pattern in front of the crack tip was

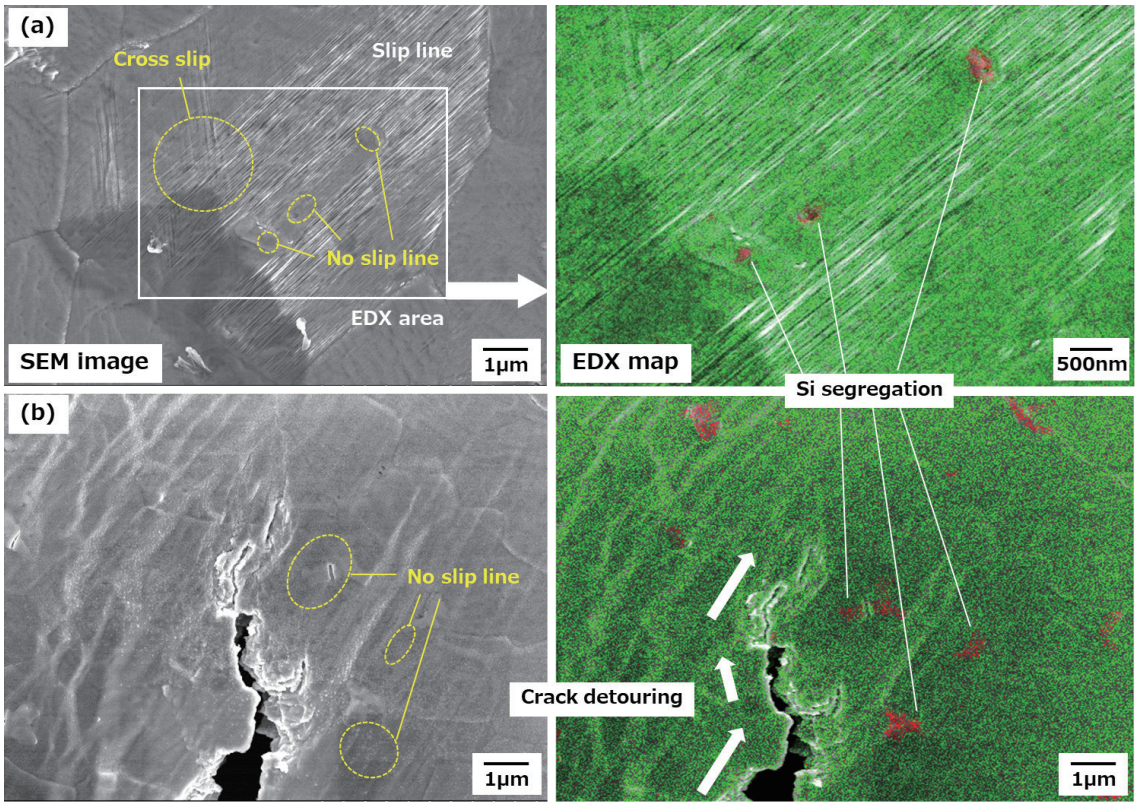

Fig. 5. (Color online) SEM and EBSD images of fatigue crack stopping and the detouring around Si segregates for zigzag cracking under dynamic tension.

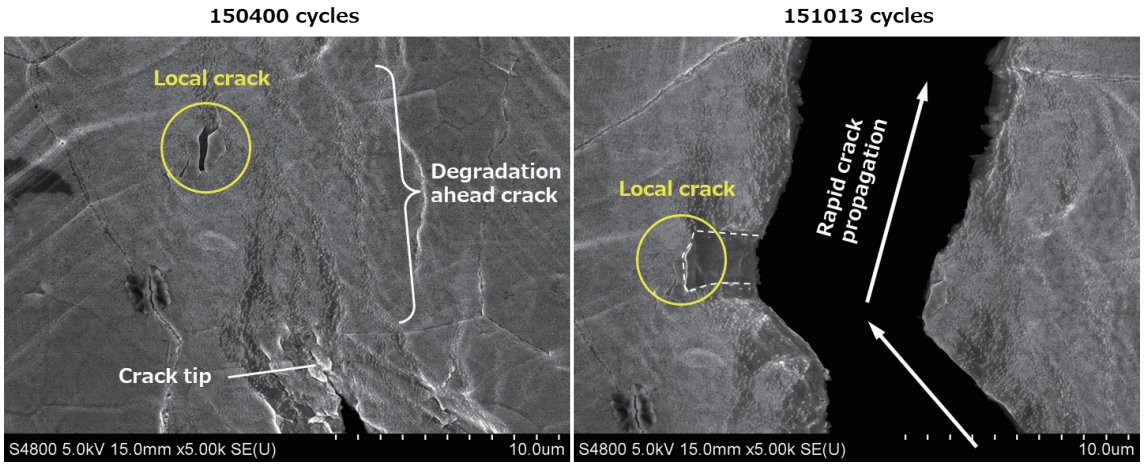

Fig. 6. (Color online) SEM images of degrading AlSi film just before fatigue failure (Detail of A in Fig. 4).

observed in the final part of the fatigue test. The mottle pattern is possibly the degradation caused by multiple short dislocation glides that happened owing to large stress concentrations originating from a fatigue crack opening process produced in the area. Also, a local crack was produced beside the mottle-pattern region. Because of Si segregation, the region might have been brittle as compared with other portions, which would have brought about a somewhat brittle fracture in the local area because a large stress was definitely concentrated around the local crack. With the combination of the two mechanisms above, consequently, in the last part of the test, the AlSi film probably catastrophically fatigue fractured, which was likely a brittle fracture, along the specimen width direction perpendicular to the loading direction.

From the crack propagation observation results, the fatigue crack in the AlSi film was found to propagate in a zigzag manner as it detoured the Si segregates. To deeply understand the effect of the Si additive on fatigue cracking in the AlSi film, the stress amplitude during the fatigue test was changed. Figure 7 shows photographs of the top surfaces of AlSi films after the fatigue test at stress amplitudes of 35, 40, and 45 MPa. At 35 MPa, it is found that a crack initiated at the edge of the specimen propagated in a zigzag manner from the cracking start to around three-fourths of the specimen width. After that, a straight crack was observed until fracture. Many slip lines were visible near the propagating crack. These trends are very similar to that shown in Fig. 4. At a stress amplitude of 40 MPa, basically, a trend similar to zigzag cracking was seen. However, the degree of the zigzag of the crack appears to be smaller than that at 35 MPa. When the stress amplitude increased to 45 MPa, the crack propagation pattern changed to straighter than the other two specimens, regardless of having multiple slip lines inclined at around 45°, which was almost the same as the other two specimens. That is, the Si additive in the AlSi film was found to be more effective for crack stopping and then detouring under the low stress amplitude condition than under the high stress amplitude one.

To understand the influence of stress amplitude on fatigue cracking in more detail, the crack path was analyzed as illustrated in Fig. 8. The photographs shown in the figure were taken before the fatigue test. The red thick lines on each photograph indicate the crack path under each condition during the fatigue test. We tried to roughly estimate the crack propagation rate during

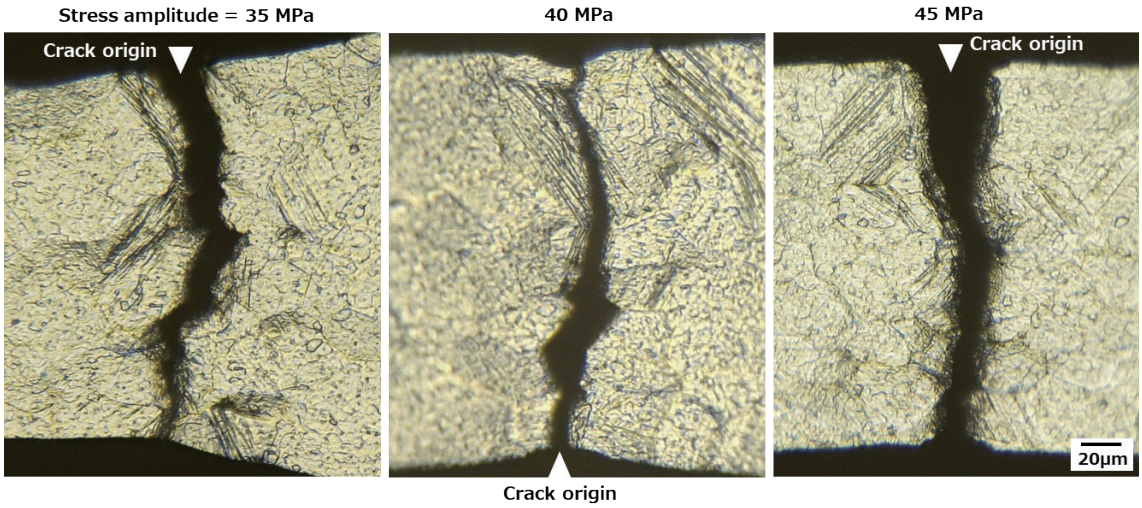

Fig. 7. (Color online) Fatigue cracking paths at stress amplitudes of 35, 40, and 45 MPa during dynamic tension loading.

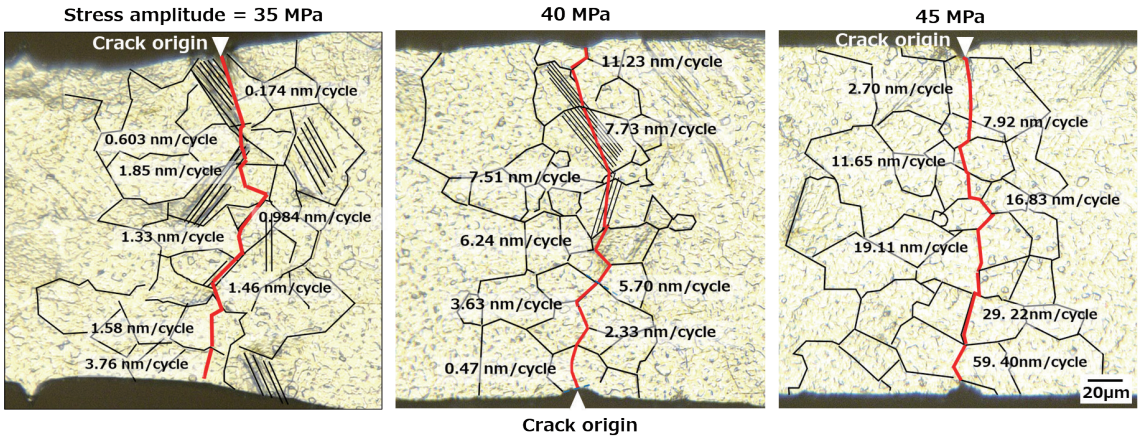

Fig. 8. (Color online) Crack path analysis in AlSi films under dynamic tension.

the tests by comparing the propagated crack length measurable from the snapshots with the number of loading cycles at the moment. All the figures in Fig. 8 include multiple information, crack path, crystal grain, grain boundary, slip lines, and crack propagation rate at the moment. At the stress amplitude of 35 MPa, the crack propagation rate was initially 0.174 nm/cycle. After that, the rate gradually increased to 1.85 nm/cycle at one-third of the specimen width. At around the middle of the specimen, the crack propagation direction considerably changed from the bottom right to the bottom left. At the moment, the propagation rate decreased slightly to 0.984 nm/cycle, around half of the last rate. In the latter half, the crack propagated to roughly the bottom-left side of the picture with increasing propagation rate. At the last moment, the rate was 3.76 nm/cycle. At 40 MPa, the initial crack propagation rate was 0.47 nm/cycle, which was 2.7

times higher than that at 35 MPa. Owing to the straighter cracking at 40 MPa than at 35 MPa, the propagation rate increased monotonically throughout the fatigue test. Immediately before fatigue fracture, the propagation rate at 40 MPa was 11.23 nm/cycle, around three times higher than that at 35 MPa. At 45 MPa, the crack propagation was faster than that under the other two conditions. At the initial and final moments, the crack propagation rates were 2.70 and 59.4 nm/cycle, respectively, which were 5.3–5.7 times higher than those at 40 MPa.

Figure 9 shows the relationship between the crack propagation rate and the propagated crack length. The circle, triangle, and squared plots indicate the stress amplitudes of 35, 40, and 45 MPa, respectively. The crack propagation rates are based on the estimation results in Fig. 8. The propagated crack length indicates the traveled distance of the crack tip from one edge to the other edge of the film specimen. At 35 MPa, in the first stage ranging from 0 to 60 μm in crack length, the crack propagation rate of the AlSi film was found to increase from around 0.2 to 1 nm/cycle. After that, in the middle stage from 60 to 180 μm in crack length, the crack propagation rate of the AlSi film was maintained at around 1 nm/cycle. In the final stage, the propagation rate rapidly increased until fatigue failure. In fact, the shape of the propagation rate–crack length relationship looks like a creep S-shaped curve. It is well known that a creep curve can be divided into three regions, primary (transient) creep, secondary (steady state) creep, and tertiary creep. On the basis of these regions, the change in crack propagation rate (fatigue degradation rate) can be explained as follows. In the first stage, a crack initiated at the specimen edge started to propagate rapidly toward the inside. The reason for the fast propagation can be as follows. The energy that accumulated around the specimen edge owing to stress concentration was released in a short period, which accelerated crack propagation. In the second stage, the

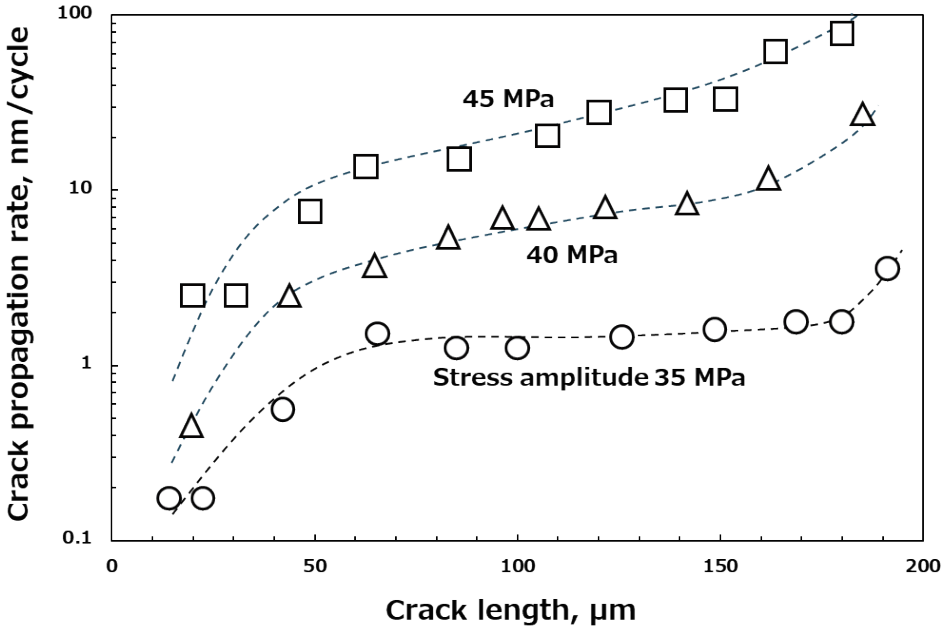

Fig. 9. Relationship between fatigue crack propagation rate and crack length.

crack propagation rate stayed almost constant because the driving forces for cracking and mechanical resistance were balanced. Actually, the crack propagated in a zigzag manner as it passed the middle section of the specimen. In the third stage, the cross-sectional area of the specimen rapidly became small, so the propagation rate increased considerably. At the stress amplitudes of 40 and 45 MPa, a trend almost similar to that observed at 35 MPa can be seen except for two things: the slope in the second stage and the crack propagation rate in every stage. At 40 MPa, the crack propagation rate in the second stage did not remain constant, but gradually increased linearly in the semi-logarithmic graph as the crack length increased. The propagation rate at 60 nm in crack length was roughly 4 nm/cycle, which increased to around 10 nm/cycle at 160 nm in crack length. At 45 MPa, the propagation rates at 60 and 160 nm in crack length were around 15 and 50 nm/cycle, respectively, which were roughly 5 times higher than that at 40 MPa at every crack length. The reason why the crack propagation rate and crack length relationship did not remain constant can be that the driving force for cracking was always greater than the mechanical resistance originating from Si segregates, as seen in the comparison between the AlSi alloy film and the pure Al film.[16] Moreover, with increasing stress amplitude, the slope of the crack propagation rate in relation to crack length increased. The AlSi alloy films used in this study contained 1 wt% Si. Si was probably distributed almost uniformly, but Si segregated portions were definitely Si rich. Si segregated portions are definitely hard mechanically because Si is harder than Al, but possibly brittle as compared with the portion with less Si. The higher stress amplitude during the fatigue test gave rise to a faster pulsating-tension loading, leading to a higher kinetic energy for crack propagation. This provided the ease of brittle-like fracture at the Si segregated portions, which would have made the Si segregates less effective in the stopping and detouring of fatigue crack under large stress amplitude conditions.

4. Conclusions

In this paper, the fatigue crack nucleation and propagation mechanisms of a sputtered AlSi alloy film were examined by the combination of quasistatic/dynamic tensile loading tests, SEM crack observations, and EBSD and EDX analyses. Quasistatic tension loading demonstrated that crystal grain subdivision happened first at the part with stress concentration. Then, dynamic tension loading demonstrated that slip lines originating from the dislocation glides formed, then crack nucleation was initiated, and then the crack started propagating along the slip lines. A crack propagated in a zigzag manner under slow loading conditions so that it stopped and then detoured Si segregates, whereas a crack propagated straightly under fast loading conditions. It was found that the balance between the driving force for cracking and the mechanical resistance around the Si segregates determined the cracking manner during the fatigue test. Si added into the AlSi film was confirmed to work well in reducing the crack propagation rate, contributing to the long-term reliability of the AlSi film.

References

1 I. Reines, B. Pillans, and G. M. Rebeiz: J. Microelectromech. Syst. **20** (2010) 193. https://doi.org/10.1109/JMEMS.2010.2090505

2 Z. Han, C. Frydendahl, N. Mazurski, and U. Levy: Sci. Adv. **8** (2022) eabn0889. https://doi.org/10.1126/sciadv.abn0889
3 K. Ruotsalainen, D. Morits, O. M. E. Ylivaara, and J. Kyynarainen: J. Opt. Microsyst. **2** (2022) 011006. https://doi.org/10.1117/1.JOM.2.1.011006
4 J. Zhang, J. Reif, C. Strobel, P. Chava, A. Erbe, A. Voigt, T. Mikolajick, and R. Kirchner: Micro and Nano Eng. **19** (2023) 100179. https://doi.org/10.1016/j.mne.2023.100179
5 T. Namazu, K. Kuwahara, M. Fujii, S. Kanetsuki, S. Miyake, and S. Inoue: Sens. Mater. **28** (2016) 141. https://doi.org/10.18494/SAM.2016.1226
6 K. Sato, M. Shikida, M. Yamasaki, and T. Yoshioka: Proc. 9th Int. Workshop Micro Electromechanical Systems (1996) 360–364. https://doi.org/10.1109/MEMSYS.1996.494008
7 T. Tsuchiya, O. Tabata, J. Sakata, and Y. Taga: J. Microelectromech. Syst. **7** (1998) 106. https://doi.org/10.1109/84.661392.
8 T. Namazu, S. Inoue, H. Takemoto, and K. Koterazawa: IEEJ Trans. Sen. Micromach. **125** (2005) 374. https://doi.org/10.1541/ieejsmas.125.374
9 Y. Isono, T. Namazu, and N. Terayama: J. Microelectromech. Syst. **15** (2006) 169. https://doi.org/10.1109/JMEMS.2005.859196
10 A. Takakura, K. Beppu, T. Nishihara, A. Fukui, T. Kozeki, T. Namazu, Y. Miyauchi, and K. Itami: Nature Commun. **10** (2019) 3040. https://doi.org/10.1038/s41467-019-10959-7
11 M. E. Saleh, J. L. Beuth, Y. N. Picard, and M. P. de Boer: J. Microelectromech. Syst. **24** (2015) 2008. https://doi.org/10.1109/JMEMS.2015.2459695
12 M. Fujii, T. Namazu, H. Fujii, K. Masunishi, Y. Tomizawa, and S. Inoue: J. Vac. Sci. Technol. B **30** (2012) 031804. https://doi.org/10.1116/1.4711040
13 T. Namazu, M. Fujii, H. Fujii, K. Masunishi, Y. Tomizawa, and S. Inoue: J. Microelectromech. Syst. **22** (2013) 1414. https://doi.org/10.1109/jmems.2013.2257985
14 A. Barrios, C. Kunka, J. Nogan, K. Hattar, and B. L. Boyce: Small Methods **7** (2023) 2201591. https://doi.org/10.1002/smtd.202201591
15 J. Koike, S. Utsunomiya, Y. Shimoyama, K. Maruyama, and H. Oikawa: J. Mater. Res. **13** (1998) 3256. https://doi.org/10.1557/JMR.1998.0442
16 M. Shindo, D. Yasugi, H. Saegusa, H. Tsuma, T. Nishiwaki, and T. Namazu: Thin Solid Films **794** (2024) 140304. https://doi.org/10.1016/j.tsf.2024.140304
17 T. Namazu: IEEJ Trans. Electrical and Electronic Eng. **18** (2023) 308. https://doi.org/10.1002/tee.23747
18 Y. Ueshima, M. Hasegawa, N. Kubota, Y. Matamura, E. Matsubara, K. Seki, and T. Hirato: Materialia **30** (2023) 101853. https://doi.org/10.1016/j.mtla.2023.101853